In-plane mode dynamics of capillary self-alignment — Supporting Information

Gari Arutinov,[†,‡] Edsger. C. P. Smits,[†] Pierre Albert,[†] Pierre Lambert,[¶] and Massimo Mastrangeli[*,¶]

Holst Centre/TNO, High Tech Campus 31, 5656AE, Eindhoven, The Netherlands, Microsystems, Eindhoven University of Technology, De Wielen, 5612 AZ, Eindhoven, The Netherlands, and Bio, Electro And Mechanical Systems (BEAMS), École Polytechnique de Bruxelles, Université Libre de Bruxelles, 1050 Bruxelles, Belgium

E-mail: massimo.mastrangeli@ulb.ac.be

This document presents the supplementary figures ($S\#$) and explanatory content referred to in the main text of the paper.

[*]To whom correspondence should be addressed

[†]Holst Centre/TNO, High Tech Campus 31, 5656AE, Eindhoven, The Netherlands

[‡]Microsystems, Eindhoven University of Technology, De Wielen, 5612 AZ, Eindhoven, The Netherlands

[¶]Bio, Electro And Mechanical Systems (BEAMS), École Polytechnique de Bruxelles, Université Libre de Bruxelles, 1050 Bruxelles, Belgium

Experimental setup

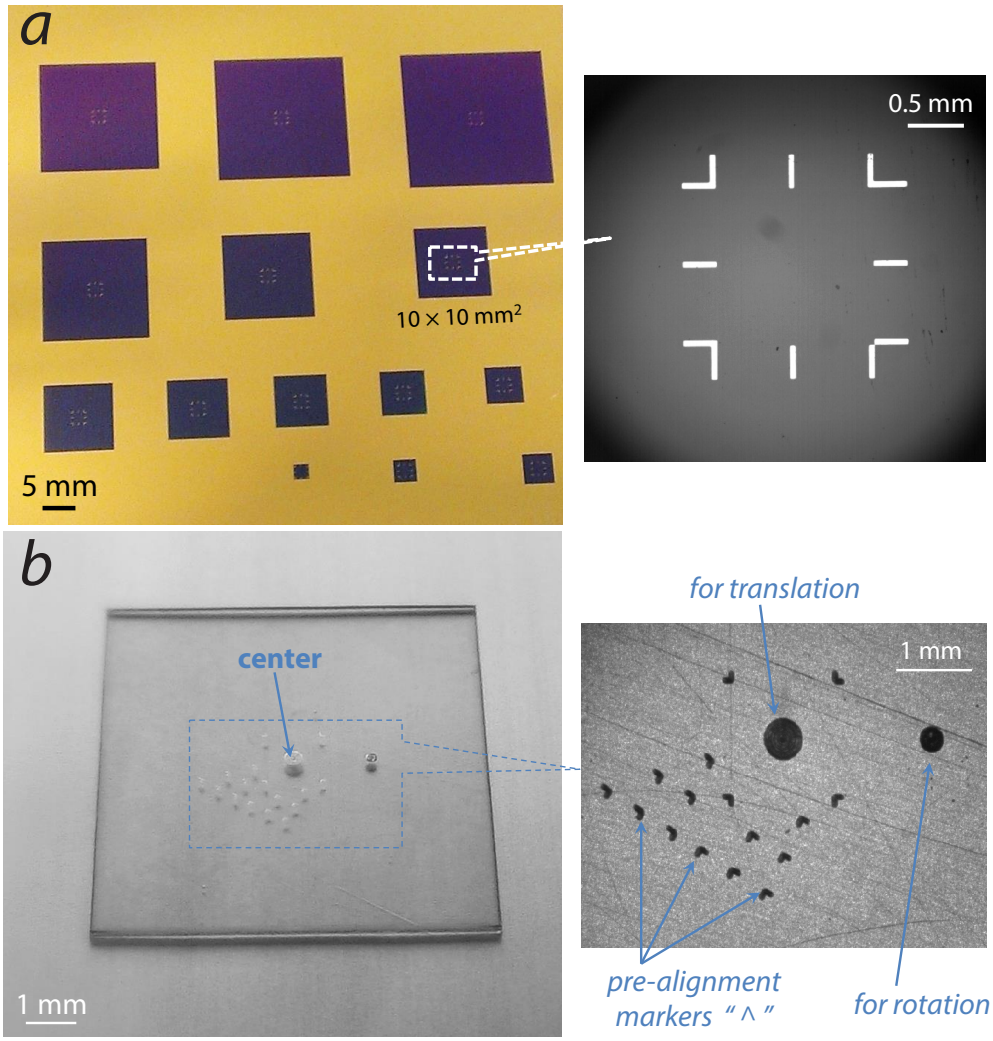

Figure S1. (a) Optical image of a Si wafer coated with a thin Au layer functionalized with perfluoro-decanethiol SAM. Dark square areas are hydrophilic SiO_2 receptor sites. Marker structures [inset of (a)] consisting of 50 μm-wide Au lines were patterned at the center of each site. (b) Optical image of a 10×10 mm^2 transparent die laser-cut from a 250 μm-thick PEN foil. The laser was also used to engrave marker structures—a reference circle in the center, a smaller circle offset to the side, and caret-like marks—on each foil die [inset of (b)]. The complementary design of the marker structures on receptor sites and transparent foil dies allows accurate simultaneous retrieval of both translational and rotational dynamics during capillary self-alignment (see Figure SF 3 for details).

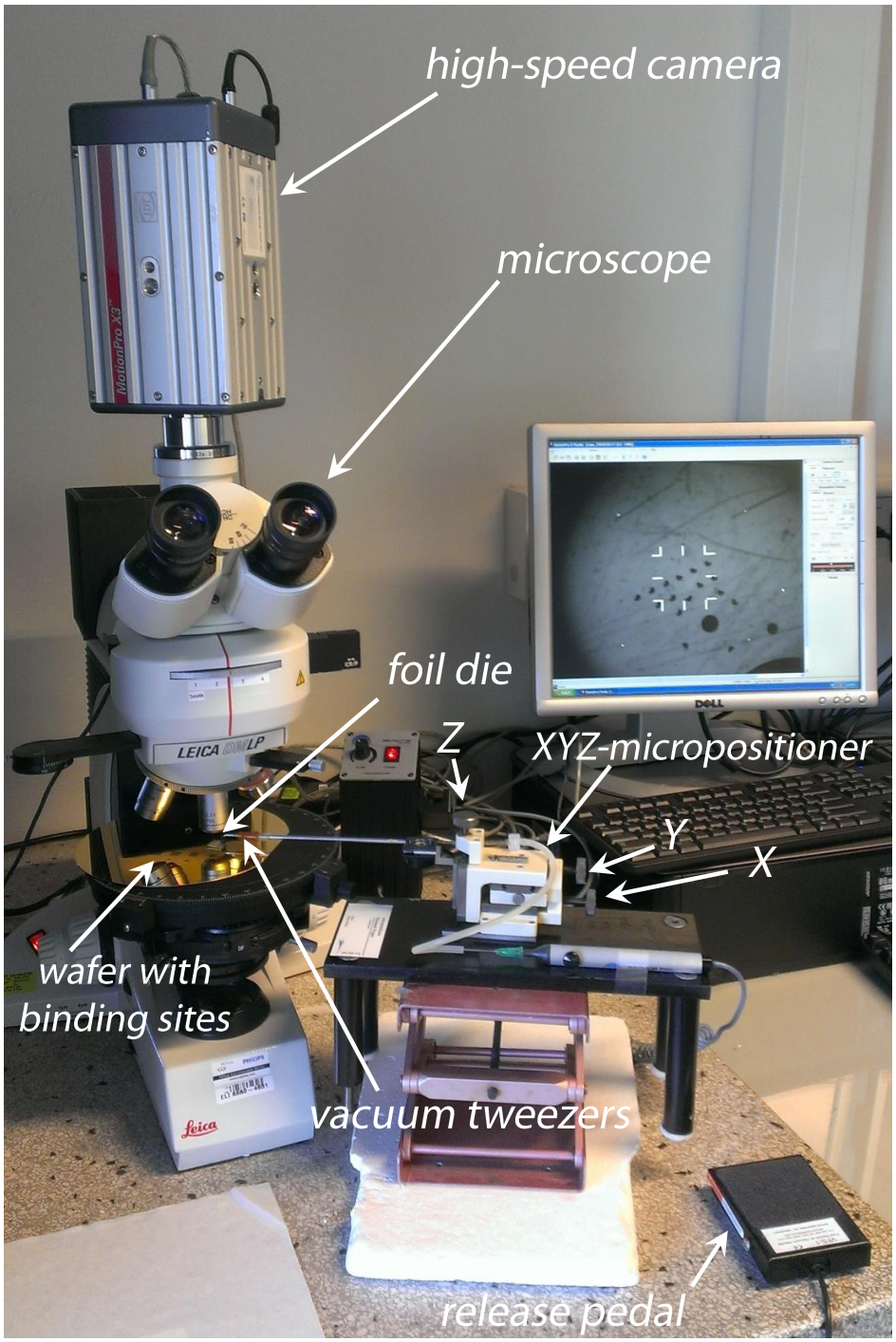

Figure S2. Experimental platform for synchronous high-resolution recording of the trajectories of self-aligning foil dies. The positioning base stage with external vacuum tweezers was used to pick up, pre-position and release the foil dies. The high-speed camera mounted on top of the microscope stage recorded in real-time the entire self-alignment process.

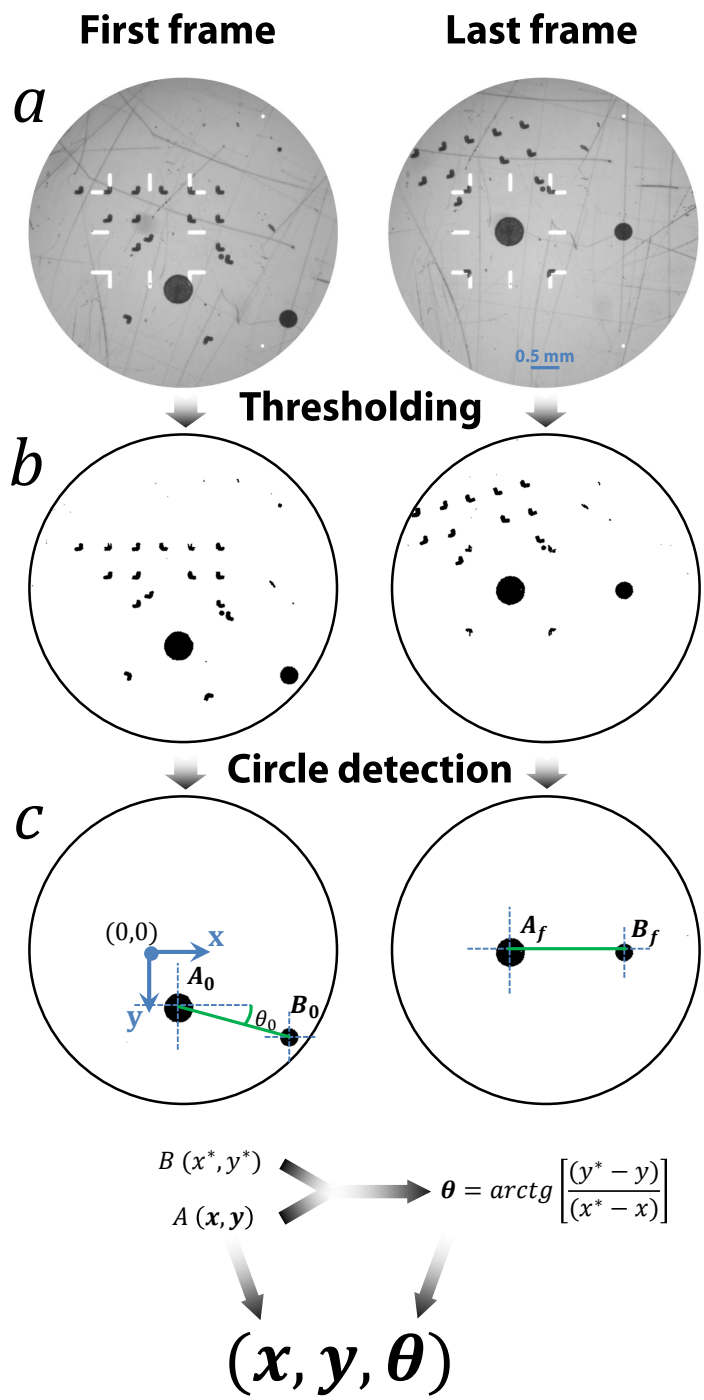

Figure S3. Retrieval of instantaneous pose (shifts $x(t)$ and $y(t)$, twist $\theta(t)$) of a die relative to the receptor site by post-processing of recorded videoframes. Raw images (a), thresholded images (b) and images with detected circles (c) shown for the first (left column) and the last (right column) of the videoframes recorded in a single experiment. Bounding circles correspond to the limit of the field of view of the microscope lens.

Decomposibility of the capillary potential field

The exact decomposition (within experimental accuracy) of the self-alignment *trajectories* under biaxial shift into individually-excited uniaxial shift trajectories in absence of initial twist offset leads to infer a structure underlying the capillary potential field $U(x,y)|_{\theta_0=0}$—whose shape was earlier computed.[1] Specifically, for in-plane translational offsets $0 \leq x_0, y_0 \ll L$, $U(x_0,y_0)|_{\theta_0=0} = U(x_0,0)|_{\theta_0=0} + U(0,y_0)|_{\theta_0=0}$ is expected to hold.

The capillary potential field can be simulated in the quasi-static (*i.e.* thermodynamic) environment provided by `Surface Evolver`. According to the above decomposition, the potential energy for a horizontal displacement $U_{diag}(\sqrt{2}x_0)$ of the top die measured along the direction of a main diagonal of the matching receptor site should coincide with the sum of the potential energy associated with its projected displacements x_0 along the coordinate axes—*i.e.*, for $x_0 = y_0$, $U(x_0,y_0) = U(x_0,0) + U(0,x_0) = 2 \cdot U_{axis}(x_0) = U_{diag}(\sqrt{2}x_0)$. Results from SE simulations, shown in figure S4, reasonably support this prediction. The relative error in the decomposition remains small ($< 5\%$) across the entire range of uniaxial (projected) shift x_0 simulated, *i.e.* up to 10% of the sidelength L. The slight energetic divergence is attributed to the slight local difference in the curvature of the liquid meniscus in the case of diagonal versus axial displacements.

Additionally, in the *full elastic* regime[2] (*i.e.* for displacements smaller than the gap) the capillary potential field for uniaxial displacement can be described by the harmonic form $U_{axis}(x_0) = \frac{1}{2}kx_0^2$, with $k = 2\gamma\frac{L}{h}$ the elastic spring constant associated to axial lateral deformations of amplitudes $x_0 < h$. For the case of a meniscus bounded by a square die and matching receptor site, as in our case, symmetry dictates the identity of axial spring constants $k_x = k_y = k$. Let's consider a two-dimensional polar coordinate system $[r\ \phi]$ centered on the receptor site, wherein an arbitrary biaxial (radial) shift (r_0, ϕ_0) can be described by its axial projections $x_0 = r_0 \cdot \cos(\phi_0)$ and $y_0 = r_0 \cdot \sin(\phi_0)$, respectively. Then, according to the above potential energy decomposition:

$$
\begin{aligned}
U(r_0) &= U(x_0, y_0) \\
&= \frac{1}{2}k_x[r_0\cos(\phi_0)]^2 + \frac{1}{2}k_y[r_0\sin(\phi_0)]^2 \\
&= \frac{1}{2}kr_0^2
\end{aligned}
\tag{1}
$$

i.e. the potential energy should only depend on the norm of radial (biaxial) shift r_0 from the equilibrium position. As a consequence, displacements of the top die along circular arcs at constant distance r_0 around the center of the receptor site (as sketched *e.g.* in Fig. 4b of the main text) should be *isoenergetic*. Figure S5 shows that SE simulations fairly support this prediction, as well. For $r_0 = 50$ µm, the deviation of the relative potential energy from the expected constant value is small ($< 2\%$) for all values of angular displacement ϕ, and reaches the maximum in corrispondence of the main diagonal direction (*i.e.* for $\phi_0 = 45°$), supposedly for marginal differences in the shape of the meniscus. Moreover, the energetic deviation is expected to decrease for smaller values of r_0.

Corollaries of the decomposibility of the capillary potential field in absence of twist offset:

1. *The axial restoring capillary forces are* mutually independent.

   Indeed: $F_x = -\frac{\partial U(x,y)}{\partial x} = -\frac{\partial U_{axis}(x)}{\partial x} = F_x(x)$, and similarly for F_y.

   See section 3.2 of the main text for additional observations on the axial forces.

2. *The shift modes of the liquid bridge can be represented by* mutually independent *springs.*

   In fact, the off-diagonal components of the Hessian of the capillary potential field (*i.e.* U_{xy} and U_{yx}) are null:

   $k_x = U_{xx} = -\frac{\partial F_x(x)}{\partial x} = -\frac{\partial^2 U(x,y)}{\partial x^2} = k_x(x)$, while $U_{xy} = \frac{\partial^2 U(x,y)}{\partial x \partial y} = 0$—similarly for k_y.

   The mechanics of the axial springs k_* is described elsewhere.[2]

From this, a lumped description of biaxial restoring capillary forces can be envisioned.

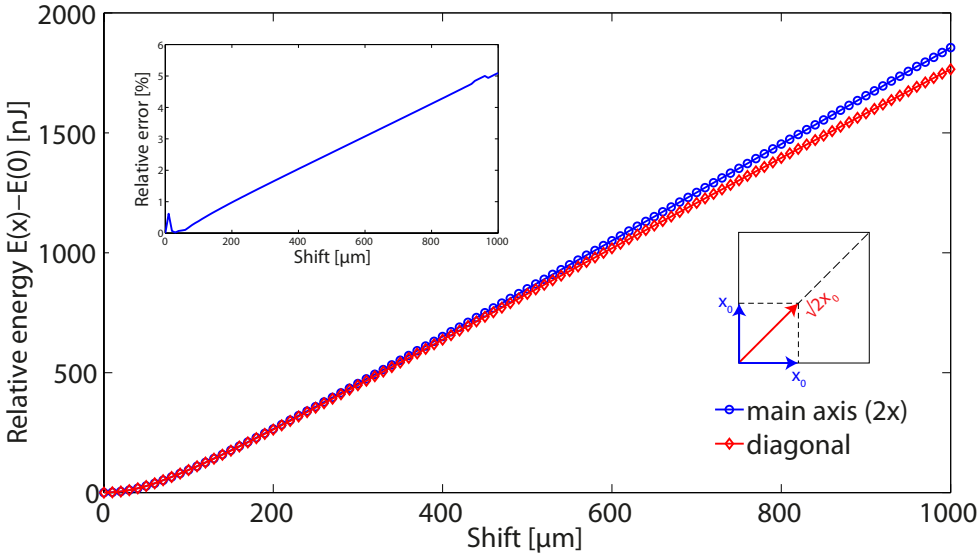

Figure S4. Decomposition of the capillary potential field $U(x, y) = U(x, 0) + U(0, y)$ in absence of twist offset. Potential energy for diagonal displacements $U_{diag}(\sqrt{2}x_0) = U(x_0, x_0)$ compared with that of the sum of the axial projections, *i.e.* $2 \cdot U(x_0, 0)$. Relative error on energy difference (see inset) computed as $|U_{diag}(\sqrt{2}x_0) - 2U(x_0, 0)|/[U_{diag}(\sqrt{2}x_0) - U(0, 0)]$.

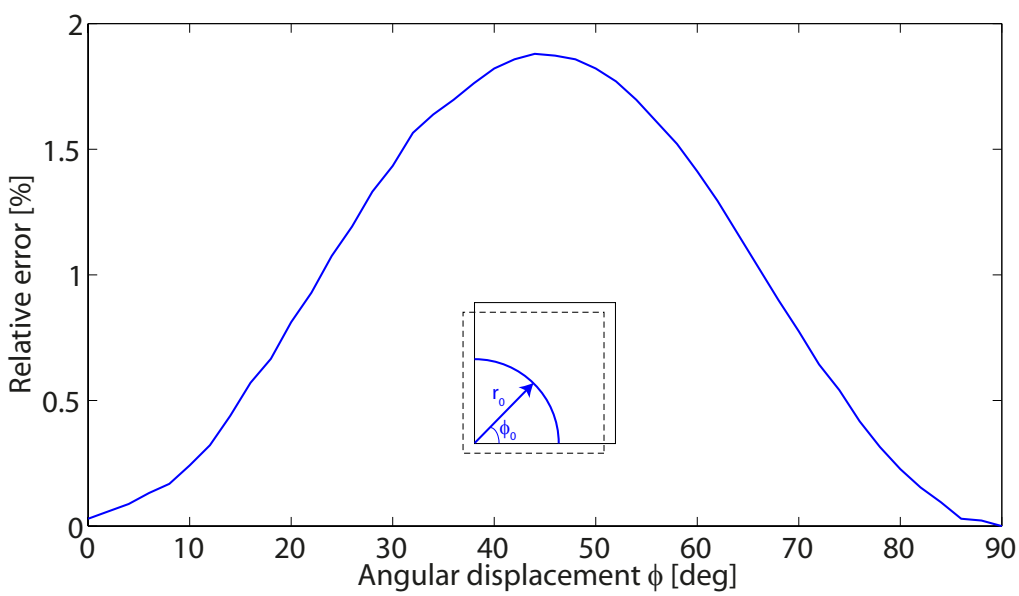

Figure S5. Decomposition of the capillary potential field $U(x, y) = U(x) + U(y)$ in absence of twist offset. Case of full elastic regime,[2] for which circular trajectories corresponding to relative displacements at constant distance r_0 (= 50 μm in this example) from the equilibrium position are expected to be isoenergetic. Relative error on the energy difference computed as $|U(r_0, \phi_0) - U(r_0, 0)|/[U(r_0, 0) - U(0, 0)]$.

The twist DOF

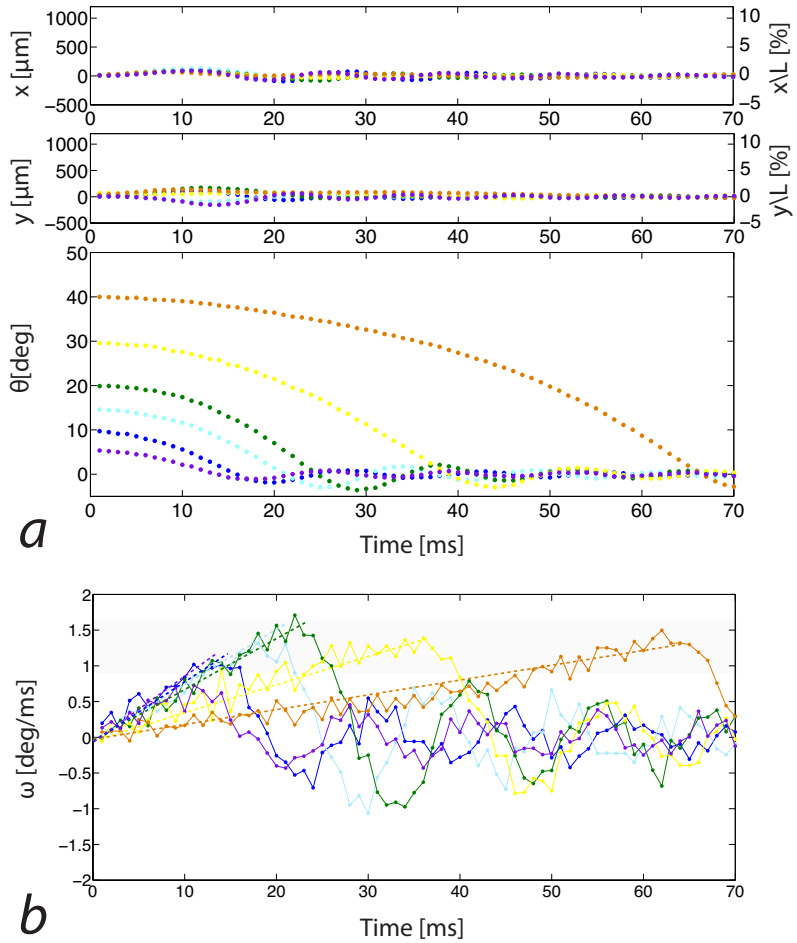

c

Angular offset [deg]	Angular acceleration [deg/ms^2]
5	0.086
10	0.081
15	0.075
20	0.067
30	0.039
40	0.021

Figure S6. The twist DOF. (a) Modal trajectories of twist dynamics for several values of initial offset ($x_0 = y_0 = 0,\ \theta_0 > 0$). (b) Corresponding die angular velocities ω along self-alignment trajectories. The values of the angular velocities for differing θ_0 tend to attain a similar maximal value. (c) Values of angular acceleration $\dot{\omega}$ numerically estimated from (b) through linear fit.

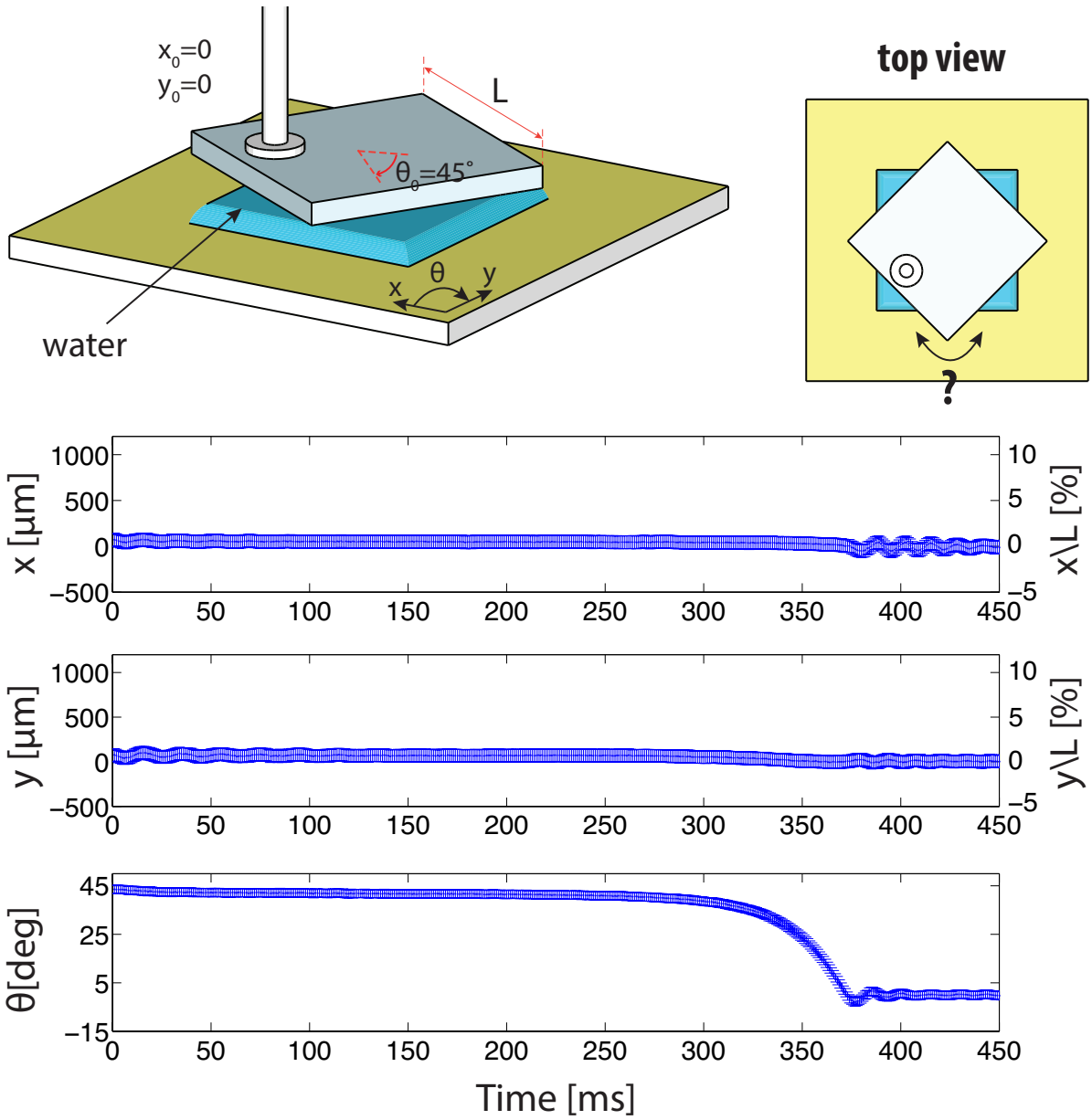

Figure S7. Rotational self-alignment dynamics for a foil die with maximal misorientation and null biaxial offset ($x_0 = y_0 = 0$, $\theta_0 = 45°$). The absence of initial capillary torque (predicted by SE simulations, see Fig. 5c in the text) causes the foil die to remain in the metastable state until the rotational symmetry is broken by vibrational noise.

Synchronisation and mode coupling

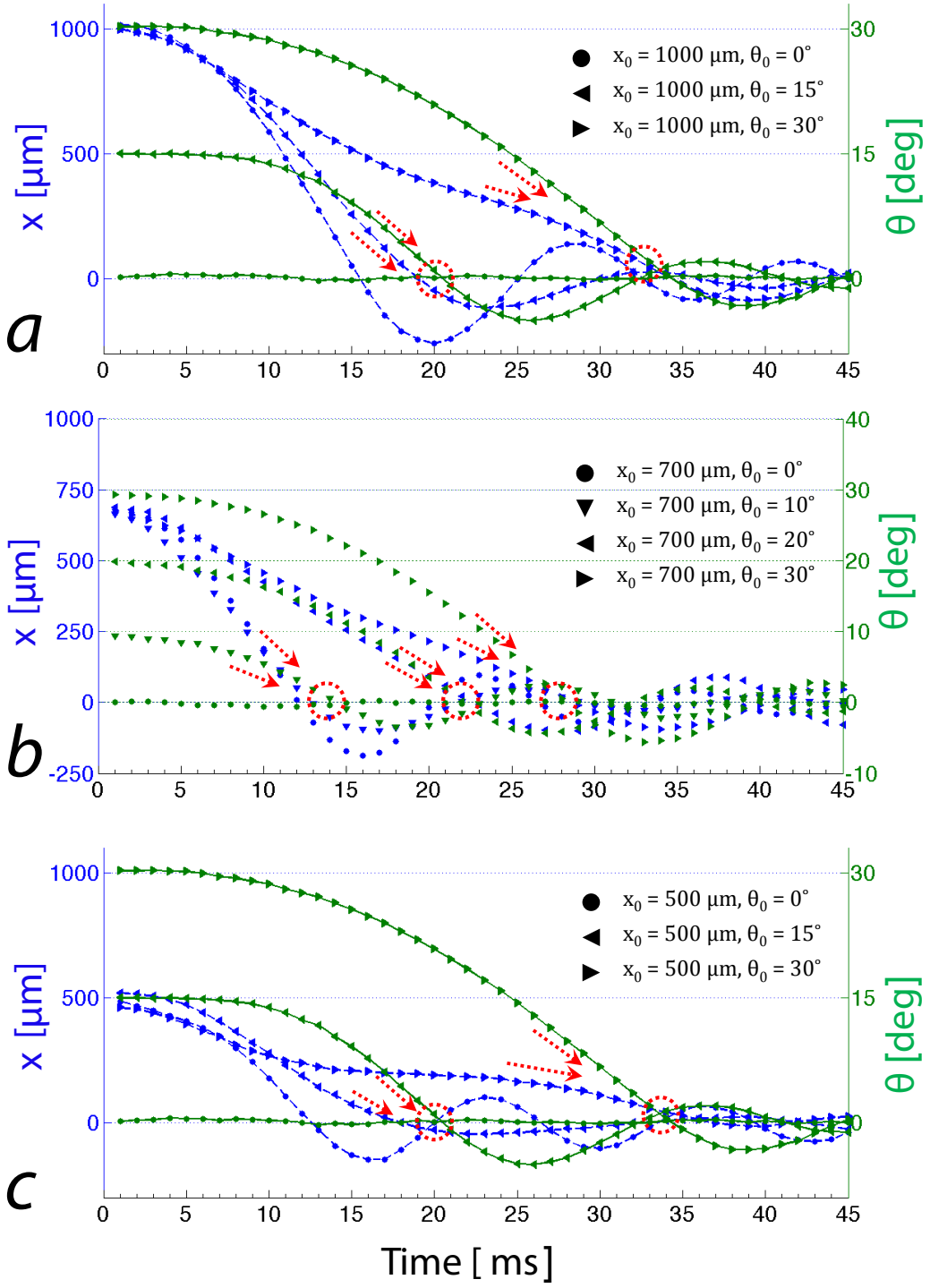

Figure S8. Alignment of times of first zero crossing in the experimental dynamics of simultaneously excited uniaxial shift and twist modes.

Non-dimensional map of self-alignment dynamics

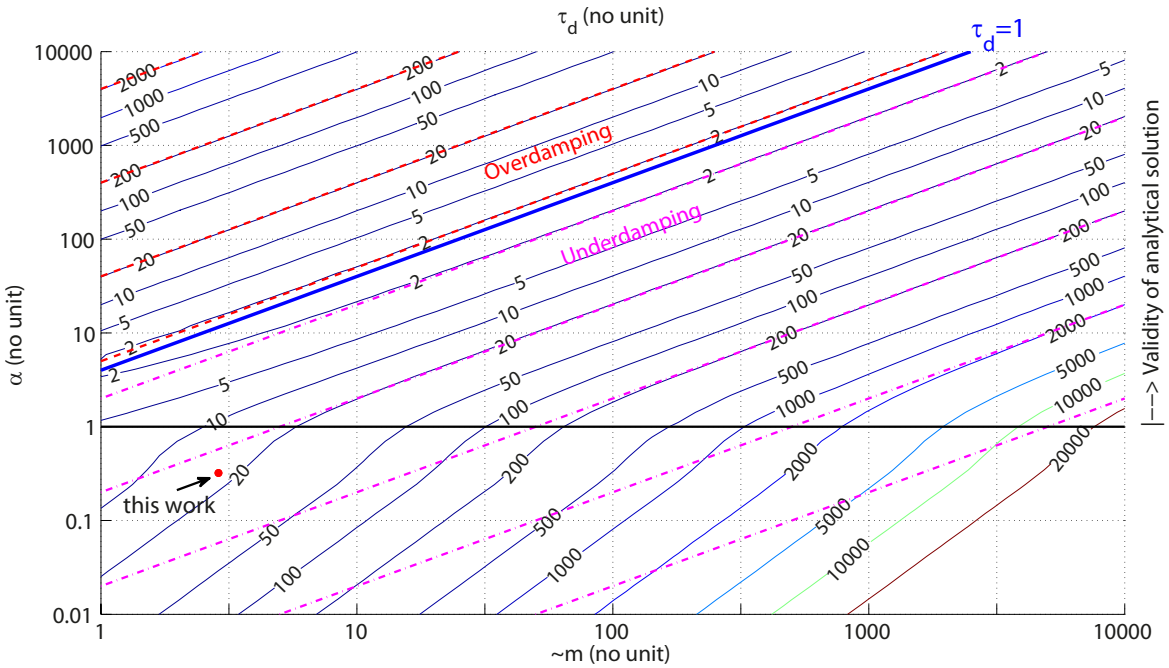

Figure S9. Map of non-dimensional damping time τ_d as function of normalized mass $\tilde{m}$ and normalized viscosity α (see text for definitions). The straight line corresponding to $\tau_d = 1$ separates the domains of overdamped and underdamped harmonic oscillations of the component. The domain above $\alpha = 1$ is the domain of strict validity of the analytical model.[3] (Adapted from Fig. 8.8 of[4] with permission from Springer Science and Business Media).

References

(1) Lienemann, J.; Greiner, A.; Korvink, J. G.; Xiong, X.; Hanein, Y.; Böhringer, K. F. In *Sensor Update 13*; Baltes, H., Fedder, G. K., Korvink, J., Eds.; Wiley-VCH, 2004; Chapter Modeling, Simulation, and Experimentation of a Promising New Packaging Technology: Parallel Fluidic Self-Assembly of Microdevices, pp 3–43.

(2) Mastrangeli, M.; Arutinov, G.; Smits, E. C. P.; Lambert, P. Modeling capillary forces for large displacements. *Microfluid. Nanofluid.* **2014**, DOI: 10.1007/s10404–014–1469–9.

(3) Lambert, P.; Mastrangeli, M.; Valsamis, J.-B.; Degrez, G. Spectral analysis and experimental study of lateral capillary dynamics for flip-chip applications. *Microfluid. Nanofluid.* **2010**, *9*, 797–807.

(4) Lambert, P., Ed. *Surface tension in microsystems*; Springer, 2013.